ESC-TR-2005-074

Technical Report
TR-1110

Performance-based Comparison of Low-Light Video Technologies for Night Surveillance

C. Fischer

3 March 2006

Lincoln Laboratory
MASSACHUSETTS INSTITUTE OF TECHNOLOGY
LEXINGTON, MASSACHUSETTS

Prepared for the Department of the Air Force under Contract FA8721-05-C-0002.

This report is based on studies performed at Lincoln Laboratory, a center for research operated by Massachusetts Institute of Technology. This work was sponsored by the Department of the Air Force, WPAFB, under Contract FA8721-05-C-0002.

The ESC Public Affairs Office has reviewed this report, and it is releasable to the National Technical Information Service, where it will be available to the general public, including foreign nationals.

This technical report has been reviewed and is approved for publication.

FOR THE COMMANDER

Gary Tutungian
Administrative Contracting Officer
Plans and Programs Directorate
Contracted Support Management

Massachusetts Institute of Technology
Lincoln Laboratory

Performance-based Comparison of Low-Light Video Technologies for Night Surveillance

C. Fischer
Group 97

Technical Report 1110

3 March 2006

Lexington Massachusetts

ABSTRACT

Differences in spectral response, pixel size, and noise characteristics between low-light video technologies complicate the direct comparison of field performance for a surveillance application. Commonly measured camera properties such as modulation transfer function and read noise do not directly relate to field performance (e.g., probability of target recognition). In modeling camera field performance based on these measured properties, many assumptions are often made such as constant prereadout gain, signal-independent noise factor, and uniform responsivity. As the imaging task approaches "photon-starved" conditions, the validity of assumptions made by commercially available modeling software becomes questionable—especially for relatively new technologies. Direct comparison of competing technologies can be used to validate modeling results, but such experiments are expensive and time-consuming, ideally requiring design, fabrication, optimization, and side-by-side testing of complete camera systems under a wide range of potential field conditions.

A proposed combined analytical and experimental method for quantitative comparison of reflective-band imaging systems will be described and demonstrated. In this method, analysis of laboratory camera measurements and field spectral irradiance measurements is used to predict field camera performance under the measured field spectral irradiance conditions. This method analytically corrects for differences in pixel size, spectral response, and noise characteristics by making assumptions about the final system design. In principle, this correction allows comparison between any two imaging technologies in the reflective-bands. The final figure of merit is the minimum human resolvable bar-target feature size (in pixels) versus night-illumination condition (e.g., quarter moon). As a practical example, the method is used to compare intensified charged coupled device (CCD) and electron-multiplied CCD cameras.

TABLE OF CONTENTS

1. INTRODUCTION

Despite many apparent advantages over the more established intensified CCD (ICCD), the newer electron-multiplying CCD (EMCCD) is rarely used in night-vision applications. The broad spectral response and low-noise characteristics make EMCCDs ideal for applications which demand low-light imaging at video frame rates. Compared to ICCD technology, EMCCDs demonstrate faster flash recovery, reduced blooming, higher optical damage threshold, and better daytime performance [1]. EMCCDs have quickly found support from many in the research community [2- 5]. Published technology comparisons are rare, often employ on laboratory lighting conditions, and occasionally come to different conclusions [5- 7]. Since spectral content of available night-illumination sources is dramatically different from most laboratory sources and the spectral response varies between technologies, these few comparisons have little relevance to night surveillance applications. Simulations based on published noise and spectral response data show significantly better performance from EMCCDs in night surveillance applications. Nevertheless, the established image intensifier technology continues to pervade most commercial night-vision products.

Three dominant system engineering challenges render EMCCD-based devices more bulky and power-hungry than their intensifier-tube equivalents. Since most night-vision devices must be man-portable, these constraints could account for the present lack of EMCCD technology in night-vision products. The first challenge is cooling. Unlike the intensifier tube, the internal electron multiplication process in EMCCDs boosts the dark current noise along with the photocurrent signal [8]. As a result, high-performance EMCCD cameras must cool the focal plane below -30°C to achieve an acceptably low level of dark current. Cooling the focal plane introduces complexity, requires additional power, and requires heat dissipation, all of which are difficult to implement in a portable device. Secondly, intensifier tubes provide an optical image as the output whereas EMCCDs require a separate display to produce an image. For most fixed or vehicle-mounted installations, a separate display is already required, but for man-portable devices the separate display adds complexity and consumes additional power. Finally, the electron multiplication process in an EMCCD requires more power than a standard CCD device or an image intensifier tube. This, in addition to the cooling and display power consumption, drives the power requirements of an EMCCD night-vision scope to several times the requirements for an image intensifier-based scope. For portable devices, additional power consumption requires a larger battery, but for fixed or vehicle-mounted sensors, the power consumption often has little or no impact.

The challenges facing EMCCD integration into portable night-vision devices are easily overcome in larger night-vision systems. However, a recent survey of six major vendors of platform-mounted night-vision turrets revealed that only one currently offers a product which uses EMCCD technology. Inspired by this anomaly and the lack of useful published comparisons between these technologies for night-vision applications, this experiment compares the relative night-time performance of these two technologies.

This experiment employs a combined experimental and analytical approach for a laboratory-based comparison of low-light video camera performance under typical night-illumination conditions. A method for cross-technology comparison is described which mathematically corrects for differences in camera spectral response and focal-plane format. Once these differences have been corrected, human perception of image quality can be measured using digitally captured images from light levels which produce the same number of photoelectrons as the desired nighttime scene. The results of this experiment lend credibility to existing low-light camera models by confirming that back-illuminated EMCCDs may offer improved performance over image intensifier-based cameras.

2. EXPERIMENTAL PROCEDURE

To compare different camera technologies in realistic night-vision scenarios, the influence of both light intensity and spectral shape must be considered. In this experiment, we have used an analytical approach to relate laboratory measurements to field conditions. The method can be broken down into five basic steps. First, field-measured spectral irradiance data are collected for several meteorological conditions representative of typical operating conditions of the system in question. Second, an optical geometry model is selected which is representative of a challenging night-vision imaging task. This geometry model is used to calculate a transfer function which converts scene spectral irradiance to spectral intensity at the focal plane of each camera. Third, the digital spectral response (*DN* per mW) of each camera is measured in the laboratory. Fourth, night spectral data are related to camera digital (*DN*) values for each camera. Finally, the camera's imaging performance can be evaluated using any light source with adjustable intensity since the camera's *DN* value is related to known night-scene conditions. This section will describe each of these steps in detail.

For the measurements described herein, typical values for night spectral irradiance were taken from data files included with the Army Night Vision Electronic Sensors Directorate's (NVESD's) SSCAM software [9]. These spectral irradiance data are shown in Figure 1. Clear nights are considered with full, quarter and, no moon. These data represent averaged spectral data from several nights collected by Roy Littleton, et al. It is important to note that the night spectral irradiance varies both in magnitude and in spectral shape with factors such as cloud cover, phase and location of the moon, solar activity, and artificial light sources. These data are an average of many nights.

Table 1 summarizes the optical geometry model used to relate scene spectral irradiance to spectral intensity at the focal plane. Since pixel size changes between cameras, the model assumes that the lens is custom designed for a particular scenario. Therefore, the lens focal length for each camera is adjusted such that the IFOV size remains constant for all cameras. This maintains the necessary number of pixels on a target of constant size and range. The lens aperture is kept constant so that the same amount of incident optical power impinges on each pixel for a given scene and range. Atmospheric and lens transmission are assumed to be independent of wavelength, weather conditions, and the parameters in Table 1.

TABLE 1

Camera and scene geometry used to convert scene spectral irradiance to spectral intensity at the camera focal plane.

Parameter (*variable*)	Value	Units
Range (r)	8	km
IFOV angle (θ)	45	μrad
Aperture (d)	10	cm
Integration time (τ)	33	ms
Atmosphere & lens transmission (T)	70%	Unitless
Average scene reflectivity (R)	37.5%	Unitless
Pixel size (l_2)	Vendor specified	μm
Focal length (f)	$f = r^2 \cdot \theta / l_2$	mm
F/#	f / d	Unitless

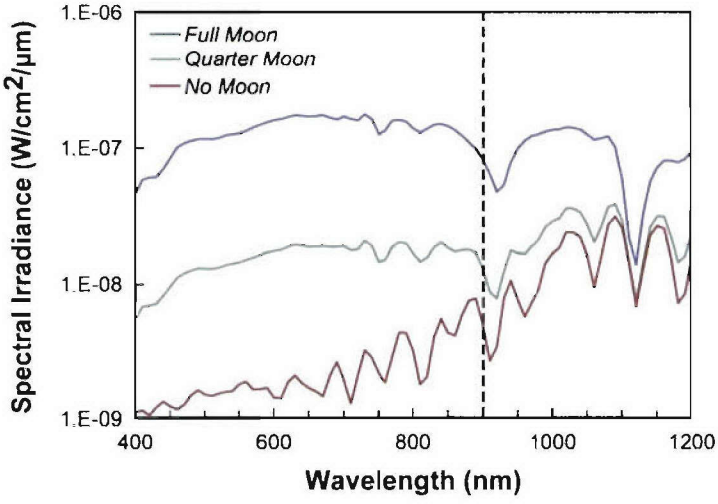

Figure 1 Spectral irradiance for several typical nighttime conditions provided by the Army Night Vision and Electronic Sensors Directorate with SSCAM. The dashed vertical line indicates the long-wavelength cut-off for generation-III filmless image intensifier tubes.

Cameras using either image intensification or electron multiplication technologies were compared; the relevant parameters for all cameras evaluated are summarized in Table 2. Spectral response of each camera's focal plane was measured. To do this, the focal plane was directly illuminated with a collimated, monochromatic light source. A small integrating sphere at the exit port of the monochromator provided spatial source uniformity. Focusing optics formed an 8-inch collimated beam. The entire apparatus (except the tungsten lamp) is contained in a dark box. Each camera was mounted such that the focal plane was illuminated in the center of the optical beam for optimal uniformity. Sets of 10 to 64 digital images were collected at several wavelengths spanning the complete spectral response of each camera. Sets of dark frames were collected at the beginning and the end of each measurement for subtraction. None of the cameras exhibited significant changes in dark counts during the spectral response measurement. A calibrated silicon photodetector was put in place of the camera focal plane to measure the incident beam intensity at each wavelength. Since several days often passed between successive camera evaluations, the spectrum of the incident beam was measured for each camera. These data were used to calculate camera digital spectral response, R_λ, according to:

$$R_\lambda = \frac{\langle DN_\lambda \rangle}{\tau \cdot L_\lambda \cdot A_{pix}}, \tag{1}$$

where $\langle DN_\lambda \rangle$ is the average DN across all pixels in the set of frames collected with the monochromator set at wavelength λ. τ is the integration time, L_λ is the wavelength-dependant intensity at the camera focal plane, and A_{pix} is the effective area of a pixel. Manufacturer's stated effective pixel size and the software-set integration time were used for A_{pix} and τ in equation (1).

The output of a single pixel in a digital camera can be calculated from the camera's digital spectral response, R_λ, the spectral intensity at the focal plane, L_λ, and pixel size A_{pix} as follows:

$$DN = \int_{\lambda 1}^{\lambda 2} R(\lambda) \cdot L_\lambda(\lambda) \cdot \tau \cdot A_{pix} \cdot d\lambda . \tag{2}$$

DN values were calculated for each camera and spectral irradiance condition. The underlying assumption made here is that the DN reported for each pixel depends only on the number of photoelectrons generated in the silicon CCD during the integration time, which in turn depends only on the spectral response and spectral shape of the illumination according to equation (1).

To evaluate each camera's imaging performance under low illumination, a chrome photomask of the USAF-1951 resolution target was used in conjunction with the collimated light source described earlier and diffuser plate to form a monochromatic, uniformly illuminated resolution chart image. The specified optical density of the chrome is greater than 3, so contrast of the resolution target should be greater than 99.9%. Differences in camera IFOVs were accommodated by normalizing bar target sizes to each camera's pixel size before comparison. Use of a monochromatic, visible light source eliminated potential chromatic dispersion and potential infrared absorption effects in the lens.

For each camera, sets of 64 images were collected at several light levels starting at high light levels where Nyquist-limited performance is observed and approaching the low-light limit of each camera. To compute the ΔDN value for a given set of images, all images in the set were averaged on a pixel-by-pixel basis. The difference between mean DN value of large light and dark regions in the final image was taken as the ΔDN value for the light level. Since each camera's digital spectral response had been measured, it was not necessary to measure the lens transmission to determine the light intensity at the focal plane. Minimum resolved bar size was observed to approach the Nyquist limit for all cameras.

TABLE 2

Camera properties, as reported in specification sheets from the respective vendors.

Property	PI Max	Photon Max	Cascade 1K
Amplification Technology	Gen-III filmless intensifier tube	Electron multiplication	Electron multiplication
Resolution	512 × 512	512 × 512	1004 × 1002
Pixel Size	24 μm (effective)	16 μm	8 μm
Sample Rate	5 MHz	10 MHz	10 MHz
Typ. read noise	50 e^-	60 e^-	15 e^-
CCD Sensor Vendor / Model	Thompson / 7895	e2v Tech. / CCD-97	Texas Inst. / TC-285
FPA Temp.	-20 °C	-55 °C	-40 °C

Once images were collected for several representative light levels, the author's ability to recognize bar patterns on the resolution target was measured. To reduce variations in human perception, three images were randomly selected for each camera at each light level. Images were viewed in random order, using a consistent spatial and contrast scaling technique. The spatial scale of the image on the display was kept greater than one to one. Mean and standard deviation of pixel values were calculated for each image and used to scale brightness and contrast such that full scale of the image spanned 4 sigma, centered about the mean pixel value. The smallest resolvable bar pattern was selected by the user and recorded by the computer for each image. After all images had been processed in this manner, the results were tabulated for each light level.

3. RESULTS AND DISCUSSION

Measured spectral response for the various cameras is similar to vendor-supplied quantum-efficiency data. Normalized spectral response curves for the three cameras are shown in Figure 2. The difference between spectral response of image intensifier tubes and CCDs is most dramatic between 900nm and 1050nm. In this spectral region, the GaAs-based generation III filmless image intensifier has no response while the silicon-based CCD continues to respond.

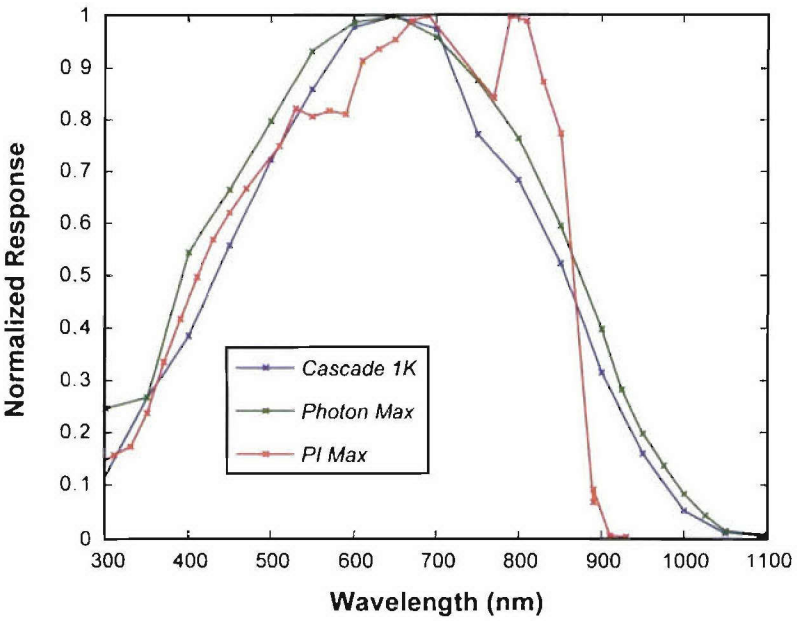

Figure 2. Normalized response of several commercial low-light cameras.

Table 3 shows *DN* values calculated from equation (2) for the camera spectral response functions shown in Figure 2, spectral irradiance data shown in Figure 1, and optical parameters given in Table 1. These values were used to relate images of the US Air Force resolution target at various light levels to realistic scenes based on measured contrast in the image.

TABLE 3

Predicted *DN* values for various cameras at "typical" light levels

Camera	Overcast Quarter Moon	No Moon	Quarter Moon	Full Moon
PI Max	9	14	93	810
Cascade 1K	52	84	520	4438
Photon Max	7	11	66	560

Minimum resolved bar frequency (normalized to the Nyquist condition) is shown as a function of light level (*DN*, normalized to full moon) in Figure 3. Since the spectral shape of scene illumination changes with atmospheric conditions, camera digital response varies between cameras and is not a linear function of moon phase. As a result, equivalent no-moon and quarter-moon light levels occur at different fractions of full-moon for each camera. Performance at these light levels is predicted based on logarithmic least-squares fits to the data. This fit is selected empirically.

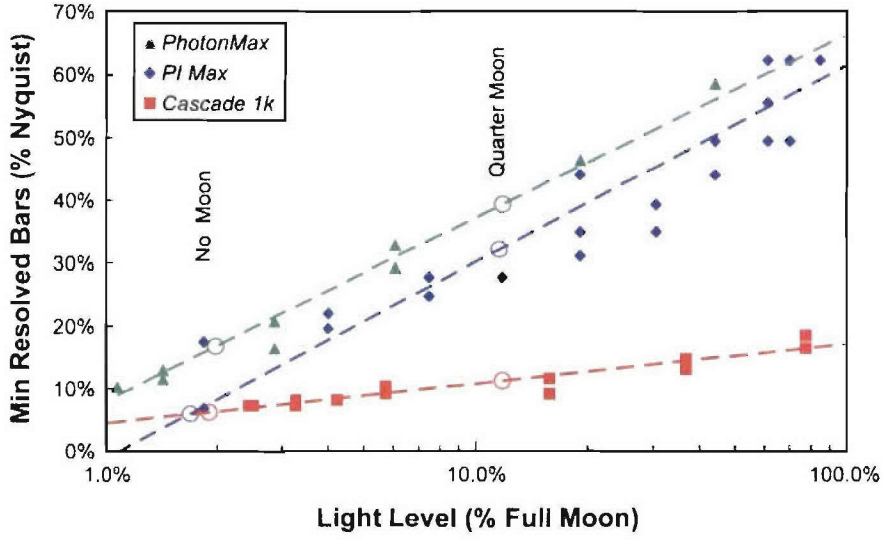

Figure 3. Camera performance. Light level is normalized to percentage of full moon. Estimated quarter-moon and no-moon performance values are indicated by circles in the appropriate gray regions. Dashed lines are logarithmic least-squares fits to the data.

The best performance is from the Photon Max EMCCD camera, followed by the PI Max image intensified CCD, and finally the Cascade 1K EMCCD. The best EMCCD and ICCD cameras compare similarly at moderate light levels, but the EMCCD camera outperforms at the lowest light levels.

Qualitatively, these results agree with low-light camera simulations performed in NVESD's SSCAM and ICCD software. Probability of recognition simulations with similar camera properties are shown in Figure 4. To compare these different measures, we consider that range at which probability of recognition falls to 50% scales approximately linearly with spatial frequency response. The ratio of EMCCD to ICCD simulated range performance (50% probability of recognition) is 2.2, whereas the ratio of experimental spatial response recognition performance is 2.8. Both methods show that the EMCCD outperforms ICCD with a significant margin. The discrepancy in these ratios likely arises from inclusion of atmospheric MTF, platform jitter, and other losses in the range simulation. These losses are not considered in the experimental approach.

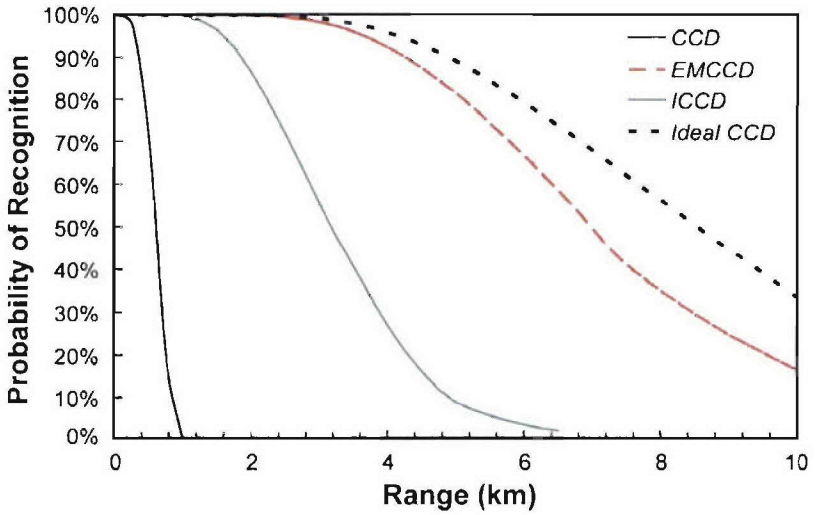

Figure 4. SSCAM and ICCD modeled probability of Recognition for imaging systems similar to that described in TABLE 1 and TABLE 2 under typical moonless night spectral irradiance. For reference, an ideal CCD system with zero read noise and an unamplified CCD with 10 electrons of rms read noise are also shown.

The poor performance of the Cascade 1K was somewhat unexpected and is not completely explained. Part of the poor performance is expected since the Cascade 1K camera uses a front-illuminated EMCCD, which has approximately 50% reduced quantum efficiency compared to the back-illuminated CCD used in the Photon Max. But poor quantum efficiency does not completely account for the measured relative performance. The smaller pixel size in the Cascade 1K could result in lens-MTF limited performance.

The PI Max performance may be slightly misstated in this comparison for two reasons. First, the focal-plane read-out rate for the PI Max is 5 MHz compared to 10 MHz for the other cameras. In general, read noise scales with read-out rate, so this difference may result in slightly overstated relative performance of the ICCD technology. Secondly, manufacturing nonuniformities result in variations in the average optical gain between image intensifier tubes. No special consideration was given to "cherry-pick" a representative image intensifier for this comparison. We believe the image intensifier used in this experiment meets manufacturer specifications. As such, it is within the range of "normal" intensifiers, but some level of uncertainty is introduced by these variations in manufacturing.

During experimentation with these cameras, several qualitative observations were made which impact performance. When any EMCCD focal plane was near room-temperature, low-light performance of the electron-multiplied output was poor. In addition to the predictable high-noise level at high temperatures, image artifacts like streaking and saturation were also observed. Additionally, fixed pattern noise was more prevalent in the EMCCD devices. Lighter pixels near the edge of the image were common, as were drifts in the average pixel value of an image during an acquisition of several frames. However, image intensifiers are susceptible to damage from intense illumination, which can result in more significant nonuniformity problems.

Back-illuminated EMCCD cameras, while offering the best overall performance, exhibited a wavelength-dependant response nonuniformity across the entire image as shown in Figure 5. This phenomenon results from back-side surface-roughness [10]. The thin-film structure of a back-illuminated CCD forms a resonant cavity. When the finesse, $\mathcal{F}$ of this cavity exceeds approximately 0.5, resonance effects become visible. Recall that finesse is defined as:

$$\mathcal{F} = \frac{\pi}{\alpha_r \cdot d} \quad , \tag{3}$$

where α_r is the (wavelength-dependant) absorption coefficient in thin-film resonator and d is the thickness of the film [11]. The peak wavelengths of the cavity modes are then given by:

$$\lambda_{\max} = \frac{2d \cdot n}{N} \quad . \tag{4}$$

Small variations in wafer thickness result in variations in the peak wavelengths of resonant optical modes across the CCD. This is manifested as spatial response nonuniformity under monochromatic illumination. The observed radial patterns in the nonuniformity are consistent with this theory, since surface roughness in these patterns is commonly observed on mechanically polished semiconductor wafers. Since the nonuniformity is wavelength dependant, it cannot be removed without *a priori* knowledge of hyperspectral scene content.

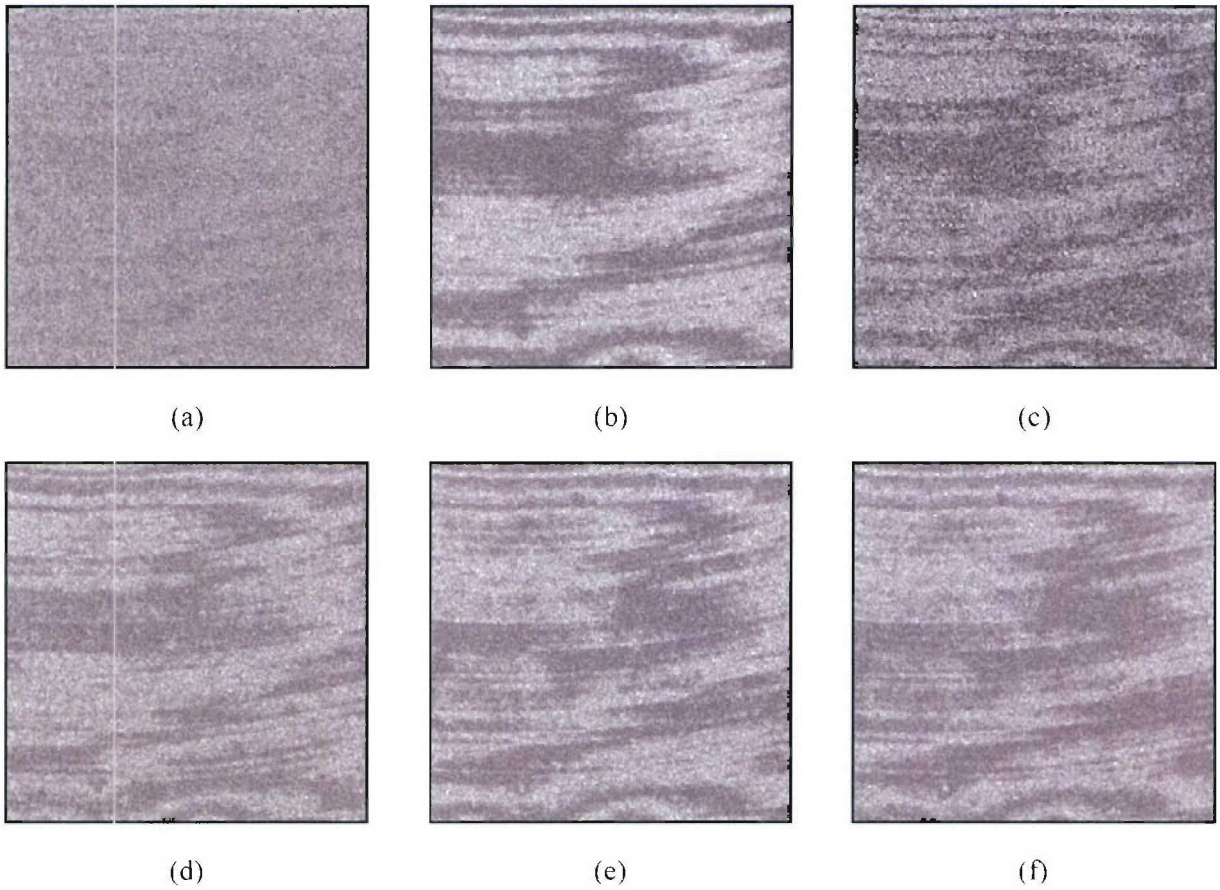

Figure 5. Digital image output from the Photon Max back-illuminated CCD for uniform illumination of wavelengths: (a) 750nm, (b) 800nm, (c) 850nm, (d) 900nm, (e) 950nm, and (f) 1000nm. Onset of spatial nonuniformity is observed between 750nm and 800nm. Images are contrast-stretched to emphasize spatial nonuniformity.

4. CONCLUSIONS

For known illumination conditions, the experimental and analytical methods presented here can be used to predict and compare performance of low-light cameras with different spectral responses and array formats. Using these methods, we have compared the performance of EMCCD and ICCD-based cameras under typical night-scene conditions. In principle, this technique can be applied to compare the performance of any imaging technology in the reflective spectral bands (visible through SWIR).

The results of this experiment suggest that EMCCDs out-perform ICCDs for typical night-illumination conditions. It appears that system engineering and integration issues centered on portable devices have thus far prevented EMCCDs from achieving widespread use in night-vision applications. These integration challenges are more easily overcome in platform-mounted night-vision systems. Besides performance, EMCCDs have several advantages over ICCDs including: broader spectral coverage, faster flash recovery, less severe blooming, higher light-damage threshold, and superior daytime performance. As a result, we conclude that the EMCCD is a good choice for the imaging sensor in larger night-vision systems.

REFERENCES

1 R. Guntupalli, V. Hagan, A. Cooper, and R. Simpson, "New ultrahigh-speed CCD camera achieves sub-electron read noise using on-chip multiplication gain (EMCCD) technology," *Proc. SPIE* 5580, 905–912 (2005).

2 P. Jerram et al., "The LLLCCD: Low Light Imaging without the need for an Intensifier," *SPIE* 4306, (2001).

3 C.G. Coates et al., "Optimizing low-light microscopy with back-illuminated electron multiplying charge-coupled device: enhanced sensitivity, speed, and resolution," *J. of Biomed. Optics* 9 (6), 1244–1252 (2004).

4 S.V. Patwardhan, S.R. Bloch, S.Achilefu, and J.P. Culver, "Time-dependent whole-body fluorescence tomography of probe bio-distributions in mice," *Optical Soc. of America* 13 (7), 2564–2577 (2005).

5 M.J. Lang, P.M. Fordyce, A.M. Engh, K.C. Neuman, and S.M. Block, "Simultaneous, coincident optical trapping and single-molecule fluorescence," *Nature Methods* 1, 133–139 (2004).

6 D. Dussault and P. Hoess, "Noise performance comparison of ICCD with CCD and EMCCD cameras," *Proc. SPIE* 5563, 195–204 (2004).

7 Andor Technology, "ICCDs edge out electron-multiplying CCDs in low light? (We don't think so!)," *Andor Tech Note – Low Light Imaging (October 2004)*, http://www.emccd.com/ICCD%20v%20EMCCD%20in%20Laser%20Focus%20World.pdf.

8 M.S. Robbins, "The noise performance of electron multiplying charge-coupled devices," *IEEE Trans. Electron. Dev.* 50 (5), (2003).

9 Hee-Sue Choi (software point of contact) and Tana Mauer (technical POC), *Solid State Camera*, US Army Communications and Electronic Command: Night Vision and Electronic Sensors Directorate, Ft. Belvoir, VA, (2002).

10 E.M. Malumuth, R.J. Hill, E.S. Cheng, D.A. Cottingham, Y.Wen, S.D. Johnson, and R.S. Hill, "Model of Fringing in the WFC3 CCDs," *Proc. SPIE* 4854, 567–576 (2003).

11 B.E.A. Saleh and M.C. Teich, "Resonator Optics," J.W. Goodman (ed.), *Fundamentals of Photonics*, New York: John Wiley & Sons (1991), Chap. 9, 310–341.